Journal of Computational and Applied Mathematics 234 (2010) 2783–2791

Contents lists available at ScienceDirect

Journal of Computational and Applied Mathematics

journal homepage: www.elsevier.com/locate/cam

A 3D non-Newtonian fluid–structure interaction model for blood flow in arteries☆

João Janela [a,b], Alexandra Moura [a,*], Adélia Sequeira [a,c]

[a] CEMAT/IST, Av. Rovisco Pais, 1, 1049-001 Lisboa, Portugal

[b] Department of Mathematics ISEG, Rua do Quelhas, 6, 1200 Lisboa, Portugal

[c] Department of Mathematics IST, Av. Rovisco Pais, 1, 1049-001 Lisboa, Portugal

ARTICLE INFO

Article history:
Received 3 March 2009
Received in revised form 18 October 2009

Keywords:
Non-Newtonian fluids
Fluid–structure interaction (FSI)
Blood flow

ABSTRACT

The mathematical modelling and numerical simulation of the human cardiovascular system is playing nowadays an important role in the comprehension of the genesis and development of cardiovascular diseases. In this paper we deal with two problems of 3D modelling and simulation in this field, which are very often neglected in the literature. On the one hand blood flow in arteries is characterized by travelling pressure waves due to the interaction of blood with the vessel wall. On the other hand, blood exhibits non-Newtonian properties, like shear-thinning, viscoelasticity and thixotropy. The present work is concerned with the coupling of a generalized Newtonian fluid, accounting for the shear-thinning behaviour of blood, with an elastic structure describing the vessel wall, to capture the pulse wave due to the interaction between blood and the vessel wall. We provide an energy estimate for the coupling and compare the numerical results with those obtained with an equivalent fluid–structure interaction model using a Newtonian fluid.

1. Introduction

Cardiovascular diseases represent a major cause of morbidity and mortality in developed countries, having a significant impact on the cost and overall status of healthcare [1]. An increasing demand from the medical community for scientifically rigorous quantitative investigations of vascular diseases, has recently given a major impetus to the development of mathematical models and numerical tools for computer simulations of the human cardiovascular system, in both healthy and pathological states. However, the circulatory system is highly integrated and modelling its various functions is an incredibly challenging problem, which requires addressing many fundamental issues, both from the mathematical and computational viewpoints [2].

Whole blood is a concentrated suspension of formed cellular elements that includes red blood cells or erythrocytes, white blood cells or leukocytes and platelets or thrombocytes. These cells are suspended in an aqueous polymer solution, the plasma, containing electrolytes and organic molecules. While plasma is nearly Newtonian in behaviour, whole blood exhibits marked non-Newtonian characteristics, mainly explained by the erythrocytes aggregation at low shear rates, their deformability and their tendency to align with the flow field at high shear rates. These complex dynamic processes contribute

☆ This work has been partially supported by the research center CEMAT/IST through FCT's funding program and by the project PTDC/MAT/68166/2006. The second author is funded by FCT through the grant SFRH/BPD/34273/2006. The authors greatly acknowledge the suggestions and remarks given by the referees, that improved the final version of this paper.

* Corresponding address: Instituto Superior Tecnico Lisboa, Center for Mathematics & Its Applications, Av. Rovisco Pais, 1, 1049-001 Lisboa, Portugal.
E-mail addresses: jjanela@iseg.utl.pt (J. Janela), alexandra.moura@math.ist.utl.pt (A. Moura), adelia.sequeira@math.ist.utl.pt (A. Sequeira).

0377-0427/$ – see front matter © 2010 Elsevier B.V. All rights reserved.
doi:10.1016/j.cam.2010.01.032

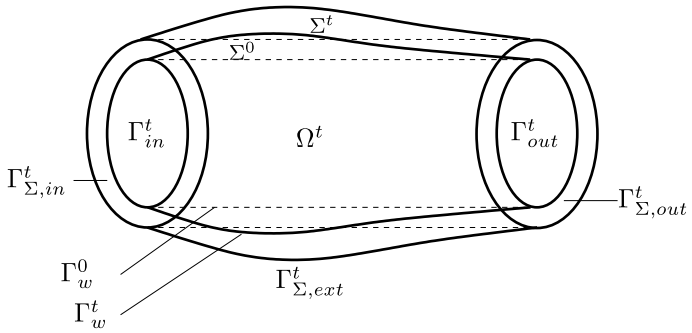

Fig. 1. Domain representing a portion of a blood vessel at time t.

to the shear-thinning, viscoelastic and thixotropic behaviour of blood. For a detailed discussion of the physical properties of blood and corresponding mathematical models see for instance [3] and references therein.

Meaningful haemodynamic simulations require constitutive models that can accurately capture the rheological response of blood over a range of physiological conditions. In most part of the arterial system of healthy individuals blood can be modelled as a Newtonian fluid (see e.g. [4,2]). However, in some disease states, namely if the arterial geometry has been altered to include regions of recirculation, detected for instance in intracranial aneurysms or downstream of a stenosis, more complex blood constitutive models should be used [5,3,6], although many authors have modelled blood flow using the Navier–Stokes equations.

Blood flow interacts mechanically with the vessel wall, giving rise to pressure waves propagating in arteries, which deform under the action of blood pressure. In order to capture these phenomena, complex fluid–structure interaction (FSI) problems must be considered, coupling physiologically meaningful models for both the blood and the vessel wall. From the theoretical point of view, this is extremely challenging because of the high nonlinearity of the problem and the low regularity of the displacement of the fluid–structure interface. So far, existence results have been obtained only in simplified cases [2]. From the numerical point of view, the use of partitioned schemes which solve iteratively the fluid and the structure sub-problems, supplied with suitable transmission conditions, is difficult to handle in haemodynamic problems, due to the large added mass effect (see [7]).

Mathematical analysis and numerical schemes for FSI problems are still largely incomplete. Most use Newtonian fluids and elasticity models ([2] and references therein), while FSI problems with non-Newtonian blood models coupled with simple or complex models for the vessel wall dynamics are practically not addressed in the literature. In this work we propose to extend existing results for 3D FSI problems with Newtonian fluids to a generalized Newtonian shear-thinning model for blood flow, using a fully implicit coupled algorithm [8]. An energy estimate for the FSI coupling will be proved at the continuous level, extending stability results already obtained in the Newtonian case [9]. Finally, numerical results are compared with those obtained with an equivalent FSI coupling using a Newtonian model for blood flow.

2. The non-Newtonian fluid model

As mentioned above, the physical properties of plasma and of the formed elements induce mechanical properties in blood that become relevant under certain flow conditions and cannot be appropriately described by the Navier–Stokes equations. It is commonly accepted that the most relevant non-Newtonian characteristic of blood is its shear-thinning behaviour (see [5, 3]). In this work we will neglect other non-Newtonian effects like viscoelasticity, thixotropy or yield-stress, and consider blood as a shear-thinning fluid described by the generalized Navier–Stokes equations.

Let $\Omega^t \subset \mathbb{R}^3$ be a bounded domain representing the space occupied by a portion of a blood vessel at time t. The part of the boundary corresponding to the physical interface is denoted Γ^t_w, while Γ^t_{in} and Γ^t_{out} represent the so-called *artificial boundaries*, that do not correspond to any physical interface (see Fig. 1). The artificial sections appear due to the truncation of the domain, since it is unfeasible to take into account the whole cardiovascular system as the computational domain.

We consider the equations for the isothermal flow of incompressible fluids, written in Eulerian coordinates, i.e. with respect to the current configuration Ω^t:

$$\begin{cases} \rho\left(\dfrac{\partial \mathbf{u}}{\partial t} + \mathbf{u}\cdot\nabla\mathbf{u}\right) - \operatorname{div}\boldsymbol{\sigma}(\mathbf{u}, P) = \mathbf{0}, & \text{in } \Omega^t,\ \forall t \in I, \\ \operatorname{div}\mathbf{u} = 0, & \text{in } \Omega^t,\ \forall t \in I, \end{cases} \tag{1}$$

where $I =]0, T]$ is the time interval and ρ is the density of blood. The unknowns are the velocity $\mathbf{u}$ and the pressure P, while $\boldsymbol{\sigma}(\mathbf{u}, P)$ is the Cauchy stress tensor, described through a constitutive relation characterizing the rheology of the fluid. In the case of Newtonian fluids the constitutive relation is simply given by $\boldsymbol{\sigma}(\mathbf{u}, P) = -P\mathbf{I} + 2\mu\mathbf{D}(\mathbf{u})$, where μ is the dynamical viscosity of blood and $\mathbf{D}$ is the strain rate tensor, given by $\mathbf{D}(\mathbf{u}) = \frac{1}{2}(\nabla\mathbf{u} + \nabla\mathbf{u}^T)$.

In this work we consider generalized Newtonian fluids, for which the viscosity is variable and depends monotonically on the rate of shear $\dot{\gamma}$:

$$\dot{\gamma} = \sqrt{\frac{1}{2}\mathbf{D}(\mathbf{u}) : \mathbf{D}(\mathbf{u})}.$$

More precisely, the generalized Newtonian model accounts for such dependence through the constitutive relation:

$$\boldsymbol{\sigma}(\mathbf{u}, P) = -P\mathbf{I} + 2\mu(\dot{\gamma})\mathbf{D}(\mathbf{u}). \tag{2}$$

Different generalized Newtonian models correspond to different specifications of the viscosity function $\mu(\cdot)$. When the viscosity decreases with the shear rate, the fluid is said to be shear-thinning (or pseudoplastic), being shear-thickening (or dilatant) when the viscosity increases with shear rate. The most common generalized Newtonian model is the power-law viscosity, given by $\mu(\dot{\gamma}) = k\dot{\gamma}^{n-1}$, where $n \in \mathbb{R}$ is the power-law index, and the parameter k is the consistency. This model became very popular because it is possible to derive analytical solutions in various flow conditions [10]. A power-law fluid is shear-thinning if $n < 1$ and shear-thickening if $n > 1$. For both mathematical and physical reasons, we will focus on bounded viscosity laws of the general form

$$\mu(\dot{\gamma}) = \mu_\infty + (\mu_0 - \mu_\infty)F(\dot{\gamma}), \tag{3}$$

where $F(\cdot)$ is a continuous monotonic function such that $\lim_{\dot{\gamma}\to 0} F(\dot{\gamma}) = 1$ and $\lim_{\dot{\gamma}\to +\infty} F(\dot{\gamma}) = 0$.

In the case of blood flow, as mentioned before, we are interested in describing a shear-thinning behaviour and therefore $\mu_0 > \mu_\infty > 0$. For this purpose we will use the Carreau–Yasuda generalized Newtonian model, which is a particular case of (3):

$$\mu(\dot{\gamma}) = \mu_\infty + (\mu_0 - \mu_\infty) \cdot (1 + (\lambda\dot{\gamma})^a)^{\frac{n-1}{a}}. \tag{4}$$

Here $\lambda > 0$, and $n, a \in \mathbb{R}$ are constants to be estimated by curve fitting of experimental data (see [11,3]). In this work we use $a = 2$, corresponding to the so-called Carreau model. The coefficients μ_0 and μ_∞ are the asymptotic viscosities, with μ_∞ the viscosity at higher shear rates, and μ_0 the viscosity for the lowest shear rates, which corresponds, in a pipe flow, to the lowest pressure drop. Notice that if $\lambda = 0$ or $n = 1$, the viscosity is constant and we recover the Newtonian model, with viscosity μ_0.

We endow equations (1)–(2) with the initial condition $\mathbf{u} = \mathbf{u}_0$, for $t = 0$, in Ω^0, while at the physical boundary Γ_w^t we impose no-slip conditions. As we will see in Section 4, this corresponds to set $\mathbf{u} = \mathbf{g}$, for $t \in I$, where the function $\mathbf{g}$ is the velocity of the structure wall, i.e. the velocity of the physical boundary, given by the model for the vessel wall dynamics. In the case of rigid vessels, where no wall displacement is considered and the domain is constant in time, we have $\mathbf{g} = \mathbf{0}$.

The prescription of proper boundary conditions on the artificial sections Γ_{in}^t and Γ_{out}^t is not a trivial task, since these conditions must account for the global effect of the remaining parts of the cardiovascular system. This issue can be handled with a geometrical multiscale approach but is not addressed in this work. For details we refer to [12,9] and references therein. Generally speaking, even if the geometrical multiscale approach is applied, we must prescribe either Dirichlet $\mathbf{u} = \mathbf{h}$, or Neumann $\boldsymbol{\sigma}(\mathbf{u}, p) = \mathbf{q}$ boundary conditions on the artificial boundaries.

3. The structure model

The vascular wall has a very complex structure, being composed of several separate layers of different materials, with distinct mechanical properties [13,14]. The derivation of appropriate and accurate constitutive models for such a complex tissue is extremely difficult and still a challenging subject of active research. Difficulties in modelling blood flow and measuring its material properties also exist for the vascular wall. Indeed, on one hand the artery wall evidences nonlinear, inelastic and stress–strain response [13,14]. On the other hand, the mechanical properties of the tissues measured in laboratory are not likely to match the ones of the same tissues *in vivo*, which poses some limitations to mechanical parameters obtained in experiments. Moreover, measurements *in vivo* are, at least for now, out of reach. Again, a balance must be found between models of high complexity, capable of describing detailed aspects of the mechanical behaviour of the material, and simpler models, less accurate but more feasible from the mathematical, numerical and computational viewpoints.

In this work we consider the 3D nonlinear model of hyperelasticity [15, Chapter 4]. Hence, the structure domain will also be a 3D bounded subset Σ^t of $\mathbb{R}^3$, varying in time. We subdivide the boundary of the structure domain Σ^t into four disjoint parts (see Fig. 1): Γ_w^t, which corresponds to the part of the boundary interfacing with the fluid domain, $\Gamma_{\Sigma,\text{ext}}^t$, which is the portion of the boundary in contact with the exterior, and $\Gamma_{\Sigma,\text{in}}^t$ and $\Gamma_{\Sigma,\text{out}}^t$, corresponding to the inflow and outflow artificial boundaries, respectively.

As it is customary in solid mechanics, we write the structure equations in the *Lagrangian* frame, i.e. with respect to a reference configuration, in cartesian coordinates. We denote by Σ^0 the structure reference domain, which is the domain at the initial time Σ^0, when the structure wall is at rest. We also assume that the reference configuration is in equilibrium, with zero internal stresses. This assumption is only an approximation for the study of blood flow in vessels, since the arterial wall exhibits a pre-stress state [13,14]. We denote by Γ_w^0, $\Gamma_{\Sigma,\text{ext}}^0$, $\Gamma_{\Sigma,\text{in}}^0$ and $\Gamma_{\Sigma,\text{out}}^0$ the corresponding reference boundaries (see Fig. 1).

The nonlinear structure model for 3D compressible elastic materials is thus given by (see [15])

$$\rho_w \frac{\partial^2 \boldsymbol{\eta}}{\partial t^2} - \mathrm{div}_0\,(\mathbf{P}) = \mathbf{0}, \quad \text{in } \Sigma^0,\ \forall t \in I, \tag{5}$$

being $\boldsymbol{\eta}$ the displacement vector with respect to the reference configuration Σ^0, ρ_w the wall density, div_0 the divergence operator with respect to the Lagrangian coordinates and $\mathbf{P} = \mathbf{P}(\boldsymbol{\eta}) = \mathbf{FS}$ the first Piola–Kirchhoff tensor, with $\mathbf{S} = \mathbf{S}(\boldsymbol{\eta})$ the second Piola–Kirchhoff tensor and $\mathbf{F} = \mathbf{F}(\boldsymbol{\eta}) = \mathbf{I} + \nabla_0 \boldsymbol{\eta}$ the deformation gradient tensor. Moreover, we denote by $\mathbf{E} = \mathbf{E}(\boldsymbol{\eta})$ the Green–St. Venant strain tensor:

$$\mathbf{E} = \frac{1}{2}\left(\mathbf{F}^T\mathbf{F} - \mathbf{I}\right) = \frac{1}{2}\left(\nabla_0^T\boldsymbol{\eta} + \nabla_0\boldsymbol{\eta} + \nabla_0^T\boldsymbol{\eta}\nabla_0\boldsymbol{\eta}\right).$$

We consider a St. Venant–Kirchhoff material [15, Section 3.9], for which the response function for the second Piola–Kirchhoff tensor is linear in $\mathbf{E}$: $\mathbf{S} = \lambda\,\mathrm{tr}(\mathbf{E})\mathbf{I} + 2\mu\mathbf{E}$, where

$$\lambda = \frac{E\xi}{(1+\xi)(1-2\xi)} \quad \text{and} \quad \mu = \frac{E}{2(1+\xi)}$$

are the Lamé constants, E is the Young modulus and ξ is the Poisson ratio.

Although the arterial wall should in principle be considered incompressible, the St. Venant–Kirchhoff model, valid in small-strain and large displacements regime, is known to perform better than the linearized models (see [15, Section 3.9]). In this study we consider a nearly incompressible material by setting a Poisson ratio close to 0.5 and a constant mass density ρ_w.

We recall that the 3D linear elastic model is obtained if instead of $\mathbf{E}$ we take its linear counterpart $\boldsymbol{e}(\boldsymbol{\eta}) = \frac{1}{2}\left(\nabla^T\boldsymbol{\eta} + \nabla\boldsymbol{\eta}\right)$.

The 3D equations of elasticity (5) have to be supplied with initial and boundary conditions. We take the initial conditions $\boldsymbol{\eta} = \boldsymbol{\eta}_0$, and $\dot{\boldsymbol{\eta}} = \dot{\boldsymbol{\eta}}_0$, for $t = 0$, in Σ^0. Since the structure equations will be coupled with the fluid model, the initial velocity $\dot{\boldsymbol{\eta}}_0$ has to be compatible with the fluid initial condition, namely $\dot{\boldsymbol{\eta}}_0 = \mathbf{u}_0$, on Γ_w^0.

Regarding the boundary conditions, at the exterior boundary we assume that the stress is zero, by taking a homogeneous Neumann boundary condition: $\mathbf{P}_0 \cdot \mathbf{n}_0 = 0$, on $\Gamma^0_{\Sigma,\mathrm{ext}}$, with $\mathbf{n}_0$ the outward normal vector to $\Gamma^0_{\Sigma,\mathrm{ext}}$. At the interface with the fluid Γ_w^0, we consider appropriate matching conditions (7), which will be introduced in Section 4 and consist of imposing the continuity of the stresses.

As for the fluid, it is not clear from physical arguments which should be the proper boundary conditions to impose on the artificial sections $\Gamma^0_{\Sigma,\mathrm{in}}$ and $\Gamma^0_{\Sigma,\mathrm{out}}$. Again, in this work we will not focus on this issue, nevertheless we refer that in this case not even the geometrical multiscale approach has provided satisfactory answers [9]. Hence, we consider a clamped structure at the extremities by setting a Dirichlet homogeneous boundary condition $\boldsymbol{\eta} = \mathbf{0}$ on $\Gamma^0_{\Sigma,\mathrm{in}} \cup \Gamma^0_{\Sigma,\mathrm{out}}$.

4. Coupling the fluid and the structure

The fluid–structure interaction problem (FSI) results from coupling the fluid equations (1)–(2) with the structure ones (5). The coupling occurs at the interface Γ_w^t, through the matching conditions between the fluid and the solid, given by

$$\mathbf{u} = \dot{\boldsymbol{\eta}}, \quad \forall t \in I,\ \text{on } \Gamma_w^t, \tag{6}$$

$$-\boldsymbol{\sigma}(\mathbf{u}, P)\cdot\mathbf{n} = \mathbf{S}(\boldsymbol{\eta})\cdot\mathbf{n}, \quad \forall t \in I,\ \text{on } \Gamma_w^t, \tag{7}$$

where $\mathbf{n}$ is the outward unit vector to Γ_w^t. Condition (7) establishes the continuity of the stresses, while (6) is the no-slip condition, that guarantees the total adherence of the fluid to the structure. The coupling is performed by imposing (6) on Γ_w^t for the fluid, and (7) on Γ_w^t for the structure (Dirichlet to Neumann coupling). Should there be an external pressure, it appears as an applied surface traction in the structure model. For the sake of simplicity, and with no loss of generality, we will consider the external pressure to be zero.

We have mentioned that the fluid equations are written in Eulerian coordinates, while the structure model is represented in a Lagrangian frame. Condition (6) is already in Eulerian coordinates, and thus ready to be imposed on the fluid equations. This is not the case of condition (7), that should be rewritten on Γ_w^0, to be prescribed on the structure model. By means of the Piola transform, we have

$$-\left(\det\nabla_{\mathbf{0}}\boldsymbol{\eta}\right)\boldsymbol{\sigma}(\mathbf{u}, P)\left(\nabla_{\mathbf{0}}^{-T}\boldsymbol{\eta}\right)\cdot\mathbf{n}_0 = \mathbf{P}(\boldsymbol{\eta})\cdot\mathbf{n}_0 \quad \text{for } t \in I,\ \text{on } \Gamma_w^0, \tag{8}$$

where $\nabla_{\mathbf{0}}$ indicates the gradient with respect to the Lagrangian coordinates, and $\mathbf{n}_0$ is the outward unit vector to Γ_w^0.

4.1. An energy estimate

In [9, Theorem 3.9] an energy estimate for the FSI coupling between the Newtonian fluid equations, written in the form

$$\begin{cases} \rho\left(\dfrac{\partial\mathbf{u}}{\partial t} + \dfrac{1}{2}\nabla|\mathbf{u}|^2 + \mathrm{curl}\ \mathbf{u}\times\mathbf{u}\right) - \mathrm{div}\ \boldsymbol{\sigma}(\mathbf{u}, P) = \mathbf{0}, & \text{in } \Omega^t,\ \forall t \in I, \\ \mathrm{div}\ \mathbf{u} = 0, & \text{in } \Omega^t,\ \forall t \in I, \end{cases} \tag{9}$$

and the structure equations (5) is proved. Here, we extend that result to the generalized Newtonian fluids in the standard formulation (1)–(2).

The FSI problem is highly nonlinear, since the solution for the fluid equations depends on the domain Ω^t, which in turn varies in time, depending on the solution $\boldsymbol{\eta}$ of the structure equations. Moreover, the solution of the structure equations depends itself on the fluid load on the vessel wall, that is, on the fluid solution. This complexity of the FSI problem makes it difficult to obtain regularity results for the coupled problem, as well as to study its well-posedness. Precisely, the 3D elastic model does not provide *a priori* sufficient regularity of the solution $\boldsymbol{\eta}$ for the coupling with the fluid equations. Indeed, from the matching condition (6), we see that the fluid velocity at the interface boundary Γ_w^t with the structure wall is given by the time derivative of the wall displacement $\dot{\boldsymbol{\eta}}$, which does not, in general, belong to $H^{1/2}(\Gamma_w^t)$, that is the natural space for the trace of the fluid solution $\mathbf{u}(t) \in \Gamma_w^t$. Several authors, in search of regularity results for the FSI Newtonian problem, add extra regularizing terms to the structure model, that however do not have a direct physical meaning [16,17]. We refer to [18] for a more recent result for strong solutions of the FSI Newtonian problem using 3D elasticity structure models.

Due to these difficulties, we assume *a priori* some regularity hypothesis, so that the integral and norms used to derive the stability result are well defined. In particular, we assume that $|\mathbf{u}(t)|^2 \in H^1(\Omega^t)$, and also that $\dot{\boldsymbol{\eta}} \in H^{1/2}(\Gamma_w^t)$, which guarantees that $\mathbf{u}(t) \in H^1(\Omega^t)$. Moreover, since the fluid domain Ω^t depends on the structure model solution, we assume that such solution is regular enough so that Ω^t is sufficiently regular at all times. In particular, we consider that, at any time $t \in \bar{I}$ the domain $\Omega^t \subset \mathbb{R}^3$ is open and connected and its boundary $\partial\Omega^t := \Gamma_w^t \cup \Gamma_{\text{in}}^t \cup \Gamma_a^t$ is locally Lipschitz (i.e., $\partial\Omega^t \in \mathcal{C}^{1,1}$).

In order to derive an energy estimate, we define the energy of the coupled FSI problem (1)–(2), (5) and (6)–(7) as

$$\mathscr{E}(t) = \frac{\rho}{2}\|\mathbf{u}\|^2_{L^2(\Omega^t)} + \frac{\rho_w}{2}\|\dot{\boldsymbol{\eta}}\|^2_{L^2(\Sigma^0)} + \mu\,\|\mathbf{E}\|^2_{L^2(\Sigma^0)} + \frac{\lambda}{2}\,\|\text{tr }\mathbf{E}\|^2_{L^2(\Sigma^0)}.$$

Proposition 4.1 (*Energy Decay Property*). *The coupled FSI problem (1)–(2), (4), (5) and (6)–(7), with homogeneous Dirichlet boundary conditions* $\mathbf{u} = \mathbf{0}$ *on* Γ_{in}^t *and* Γ_{out}^t, *satisfies the following energy inequality:*

$$\frac{\mathrm{d}}{\mathrm{d}t}\left(\mathscr{E}(t)\right) + 2\mu_\infty\|\mathbf{D}(\mathbf{u})\|^2_{L^2(\Omega^t)} \leqslant 0, \tag{10}$$

from which we obtain the energy decay property:

$$\mathscr{E}(t) + 2\mu_\infty\int_0^t \|\mathbf{D}(\mathbf{u})\|^2_{L^2(\Omega^t)}\mathrm{d}t \leqslant \mathscr{E}(0), \tag{11}$$

where $\mathscr{E}(0)$ *depends only on the initial data* $\mathbf{u}_0$, $\boldsymbol{\eta}_0$ *and* $\dot{\boldsymbol{\eta}}_0$.

Proof. As in [9, Theorem 3.9], multiplying the structure equation (5) by $\dot{\boldsymbol{\eta}}$ and integrating over the reference domain Σ^0, we obtain, due to the homogeneous boundary conditions considered for equations (5) on $\Gamma^0_{\Sigma,\text{ext}} \cup \Gamma^0_{\Sigma,\text{in}} \cup \Gamma^0_{\Sigma,\text{out}}$, and to the matching condition (7),

$$\frac{\rho_w}{2}\frac{\mathrm{d}}{\mathrm{d}t}\|\dot{\boldsymbol{\eta}}\|^2_{L^2(\Sigma^0)} + \frac{\lambda}{2}\frac{\mathrm{d}}{\mathrm{d}t}\|\text{tr }\mathbf{E}\|^2_{L^2(\Sigma^0)} + \mu\frac{\mathrm{d}}{\mathrm{d}t}\|\mathbf{E}\|^2_{L^2(\Sigma^0)} = -\int_{\Gamma_w^t}(\boldsymbol{\sigma}(\mathbf{u},p)\cdot\mathbf{n})\cdot\mathbf{u}\,\mathrm{d}\gamma. \tag{12}$$

Similarly, for the fluid equations, we multiply the momentum equation by $\mathbf{u}$ and integrate over Ω^t. Due to (6) and the Reynolds transport theorem, we have

$$\rho\int_{\Omega^t}\frac{\partial\mathbf{u}}{\partial t}\mathbf{u}\,\mathrm{d}\omega = \int_{\Omega^t}\rho\frac{1}{2}\frac{\partial}{\partial t}|\mathbf{u}|^2\,\mathrm{d}\omega = \frac{\rho}{2}\frac{\mathrm{d}}{\mathrm{d}t}\|\mathbf{u}\|^2_{L^2(\Omega^t)} - \frac{\rho}{2}\int_{\Gamma_w^t}|\mathbf{u}|^2\mathbf{u}\cdot\mathbf{n}\,\mathrm{d}\gamma. \tag{13}$$

Regarding the convective term we have, using integration by parts,

$$\rho\int_{\Omega^t}(\mathbf{u}\cdot\nabla)\mathbf{u}\cdot\mathbf{u}\,\mathrm{d}\omega = -\frac{\rho}{2}\int_{\Omega^t}|\mathbf{u}|^2\,\text{div }\mathbf{u}\,\mathrm{d}\omega + \frac{\rho}{2}\int_{\partial\Omega^t}|\mathbf{u}|^2\mathbf{u}\cdot\mathbf{n}\mathrm{d}\gamma. \tag{14}$$

We now remark that, for a shear-thinning generalized Newtonian fluid with a viscosity law (3), we have:

$$\mu_\infty \leqslant \mu(\dot{\gamma}) \leqslant \mu_0.$$

Thus, noticing that $\mathbf{D}(\mathbf{u}) : \nabla\mathbf{u} = \mathbf{D}(\mathbf{u}) : \mathbf{D}(\mathbf{u}) \geqslant 0$, we may write

$$\int_{\Omega^t} 2\mu(\dot{\gamma})\mathbf{D}(\mathbf{u}) : \nabla\mathbf{u}\,\mathrm{d}\omega \geqslant 2\mu_\infty\|\mathbf{D}(\mathbf{u})\|^2_{L^2(\Omega^t)}.$$

Finally, summing (12), (13) and (14) and considering the incompressibility condition div $\mathbf{u} = 0$, we get

$$\frac{\mathrm{d}}{\mathrm{d}t}\left(\mathscr{E}(t)\right) + 2\mu_\infty\|\mathbf{D}(\mathbf{u})\|^2_{L^2(\Omega^t)} + \frac{\rho}{2}\int_{\Gamma_{\text{in}}^t\cup\Gamma_{\text{out}}^t}|\mathbf{u}|^2\mathbf{u}\cdot\mathbf{n}\mathrm{d}\gamma \leqslant \int_{\Gamma_{\text{in}}^t\cup\Gamma_{\text{out}}^t}(\boldsymbol{\sigma}(\mathbf{u},P)\cdot\mathbf{n})\cdot\mathbf{u}\,\mathrm{d}\gamma, \tag{15}$$

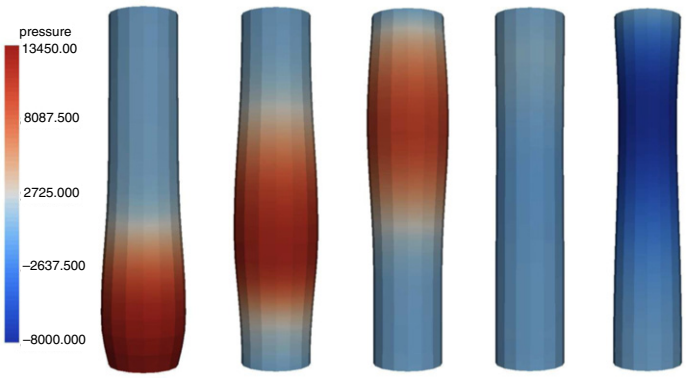

Fig. 2. A 3D representation of the pressure distribution and computational domain at times $t = 0.003$ s (left), $t = 0.006$ s, $t = 0.009$ s, $t = 0.012$ s and $t = 0.015$ s (right).

which leads to the energy inequality (10) by taking homogeneous Dirichlet boundary conditions on Γ^t_{in} and Γ^t_{out}. The energy decay property (11) is obtained integrating (10) between 0 and t, with $t \leqslant T$. ■

If instead of homogeneous Dirichlet conditions on Γ^t_{in} and Γ^t_{out}, homogeneous Neumann conditions are considered, the result holds true only if $\int_{\Gamma^t_{\text{in}} \cup \Gamma^t_{\text{out}}} |\mathbf{u}|^2 \mathbf{u}\cdot\mathbf{n} \mathrm{d}\gamma > 0$, which can be verified for instance if $\int_{\Gamma^t_{\text{in}}} |\mathbf{u}|^2 \mathbf{u}\cdot\mathbf{n} > 0$ and $\int_{\Gamma^t_{\text{out}}} |\mathbf{u}|^2 \mathbf{u}\cdot\mathbf{n} > 0$. These conditions are satisfied if the boundaries Γ^t_{in} and Γ^t_{out} are both outflow sections, meaning that the flux exits the domain: $\mathbf{u}\cdot\mathbf{n} > 0$. This is not true in general for blood flow, not even if Γ^t_{out} is a downstream section (the one closer to the systemic circulation), due to the pulsatile nature of blood flow in arteries. One way to overcome this problem is to reformulate the fluid equations as in Eq. (9) (see [9]), which can be straightforwardly applied to the equations for the generalized Newtonian fluids (1)–(2), since it does not alter the constitutive relation term of the equations. From this point of view, and after the demonstration of Proposition 4.1 presented here, the results in [9] can be easily extended to the generalized Newtonian case.

5. Numerical simulations

The numerical methods

The numerical approximation of the FSI coupling problem is performed through a splitting strategy, where the fluid and solid sub-problems are solved separately in an iterative way [19,8]. The nonlinear fluid–structure iterative coupling is performed through a quasi-Newton algorithm adapted from [8]. Here the Fréchet derivative of the fluid operator is computed exactly, while the shape derivative is approximated by the one of a Newtonian fluid.

The fluid equations are discretized in time by the implicit Euler scheme, being the nonlinear convective term linearized in a semi-implicit way: $(\mathbf{u}^n\cdot\nabla)\mathbf{u}^{n+1}$, with $\mathbf{u}^n$ and $\mathbf{u}^{n+1}$ the velocity solutions at the previous and current time steps, respectively. Also the viscous term is treated in a semi-implicit way: $\boldsymbol{\sigma}(\mathbf{u}^{n+1}, P^{n+1}) = -P^{n+1}\mathbf{I} + 2\mu(\dot{\gamma}^n)\mathbf{D}(\mathbf{u}^{n+1})$, i.e., the viscosity at the current time step is computed from the velocity gradient at the previous one. In order to account for the evolution of the computational domain, we apply the Arbitrary Lagrangian Eulerian (ALE) formulation to follow the fluid–structure interface movements (see for instance [20], and references therein). The ALE method is based on the construction of an appropriate mapping $\mathcal{A}^t : \Omega^0 \to \Omega^t$, $(\hat{\mathbf{x}}, t) \mapsto \mathbf{x} = \mathcal{A}^t(\hat{\mathbf{x}})$, from the reference domain Ω^0, to the current one Ω^t. This technique allows to overcome the mismatch on the coordinate systems between the fluid (Eulerian coordinates) and the solid (Lagrangian coordinates), by simply reformulating the Eulerian time derivative of the fluid momentum equations into the ALE time derivative: $\frac{\partial \mathbf{u}}{\partial t} = \frac{\partial \mathbf{u}}{\partial t}\big|_{\hat{\mathbf{x}}} - (\mathbf{w}\cdot\nabla)\mathbf{u}$, with $\mathbf{w} = \frac{\partial \mathcal{A}^t}{\partial t} \circ (\mathcal{A}^t)^{-1}$ the domain or mesh velocity in the current configuration Ω^t. In particular $\mathcal{A}^t := \mathbf{I}_{\Omega^0} + \boldsymbol{\eta}^f$, where $\boldsymbol{\eta}^f = Ext(\boldsymbol{\eta}|_{\Gamma^0_w})$, being Ext an arbitrary extension of the solid displacement $\boldsymbol{\eta}$ over the fluid reference domain Ω^0, which in this work is simply an harmonic extension of the fluid domain, imposed through condition (6). The fluid space discretization is carried out by means of a streamline diffusion finite element method [21,22].

Remark 5.1. At the continuous level the ALE description of the fluid is not necessary, since the change of information between the reference and current domains is carried out at each $t \in I$ in a transparent way. This is not the case anymore at the discrete level, where the time discretization calls for the use of quantities at previous time steps, when the mesh nodes were at different positions. The ALE time derivative is an adequate tool to follow the evolution of quantities associated to the moving mesh nodes.

The fluid normal stress on the fluid–structure interface Γ^t_w, prescribed on the structure equations (condition (7)), is computed in a weak form, by evaluating the residual of the fluid equations for the non-vanishing test functions on the

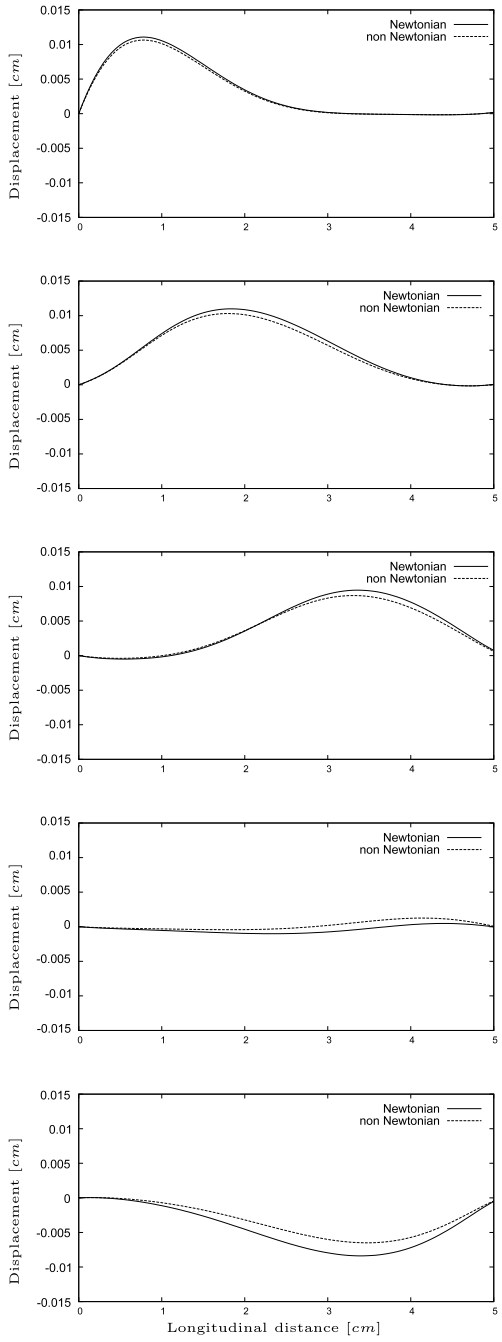

Fig. 3. Comparison of the wall displacement in a longitudinal cut at several time steps: $t = 0.003$ s (top), $t = 0.006$ s, $t = 0.009$ s, $t = 0.012$ s, and $t = 0.015$ s (bottom), for the Newtonian model (solid lines) and for the non-Newtonian Carreau model (dashed lines).

interface. The structure equations are discretized in time with the mid-point Newmark method, and in space through P1 finite elements.

Numerical results

In order to test the fluid–structure coupling described in Section 4 we setup a simple model problem. The initial fluid domain is a cylinder of radius $R = 0.5$ cm and height 5 cm, while the initial structure domain is a cylindrical shell with 0.1 cm of thickness surrounding the fluid domain. The vessel wall is described as an elastic material governed by Eq. (5), with density $\rho_w = 1.2$ g cm^{-3}, and blood is modelled as a generalized Newtonian Carreau–Yasuda fluid with density $\rho = 1.06$ g cm^{-3}

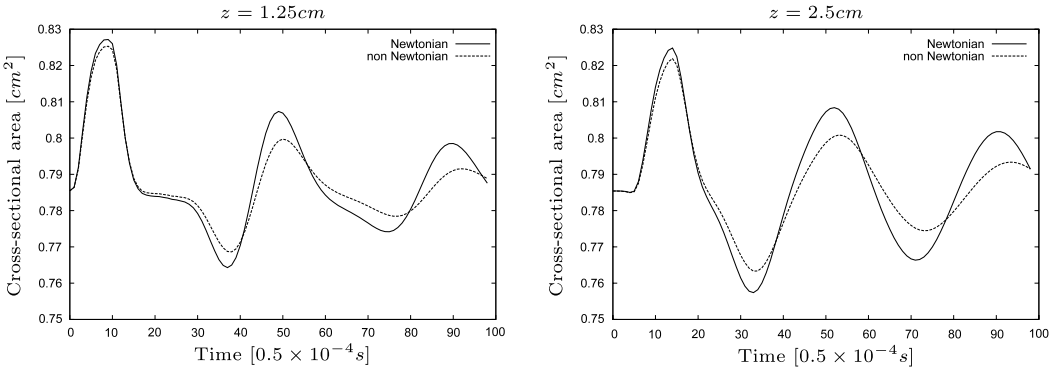

Fig. 4. Time evolution of the cross-sectional area in two different cross-sections ($z = 1.25$ cm, left, and $z = 2.5$ cm, right) for the Newtonian model (solid lines) and for the non-Newtonian Carreau model (dashed lines).

and parameters $a = 2$ (Carreau model), $\mu_0 = 0.56$ Poi, $\mu_\infty = 0.0345$ Poi, $\lambda = 3.313$ s and $n = 0.3568$ taken from [23], and, for the purpose of comparison, blood is also modelled as a Newtonian fluid with constant viscosity $\mu = 0.035$ Poi. In fact, the proper choice of the Newtonian model to compare with the generalized Newtonian models requires some caution, as described for example in [6], leading to an *a priori* choice of an equivalent Newtonian viscosity. The fluid domain is meshed with 9120 linear tetrahedral elements ($h_{\max} = 0.25$), and the structure with 3840 linear tetrahedral elements ($h_{\max} = 0.25$). The two meshes are conforming. The time step is $\Delta t = 5 \times 10^{-4}$ s.

The flow is driven by a pressure pulse generated by a constant pressure difference between the extremities of the vessel from time $t = 0$ s to $t = 0.009$ s. The vessel inflates, initially near the inflow boundary, and then the motion propagates along the vessel until it reaches the outflow section and is reflected back (see Fig. 2). This reflection is totally unphysical and is due to the use of inappropriate boundary conditions. This issue can be solved through geometrical multiscale methods (see [9]) but, in the present work, we are more interested in the stability of the coupling and not in the agreement with some given physiological data. As energy is dissipated, the motion of the wall is damped. The coupling was found to be stable, which indicates that the discrete analog of the energy inequality (4.1) holds for the particular time and space discretization described in the previous subsection.

In more detail, Fig. 3 compares the wall displacement in different time steps, both for the non-Newtonian and the Newtonian models. We can observe that there is a visible difference between both models, already in the initial time step. Since the pressure gradient and consequently the maximum shear rate, are high in the initial period, the non-Newtonian viscosity is close to the high shear viscosity μ_∞, and the behaviour is almost Newtonian, in the section of the vessel where the displacement is higher. As time advances, the differences become more visible due to accumulation of the small initial differences that result in larger discrepancies, and also because the decrease of the shear rate makes the non-Newtonian effects more prominent.

Fig. 4 illustrates the evolution of the cross-sectional area in two cross-sections: $z = 1.25$ (close to the inflow boundary) and $z = 2.5$ (middle of the vessel). The cross-sectional area in the proximal cross-section (left) appears less regular due to reflections caused by the clamping of the vessel. In both cases the amplitude of the variation of the area is damped over time, and the differences between the models become more significant as we go further away from the initial pressure pulse.

6. Conclusions

The techniques usually employed to perform 3D FSI simulations with Newtonian fluids can be extended, in a relatively straightforward way, to the case of generalized Newtonian fluids. At the continuous level, an energy estimate for the FSI coupling was demonstrated, extending the stability results given in [9]. From the numerical point of view, the coupling is stable for the test case studied here and the numerical results are coherent with the ones obtained in the Newtonian case. Even in simple test problems it is already possible to find significant differences in the velocity fields and vessel wall displacement when we use non-Newtonian or equivalent Newtonian models. We do not claim that non-Newtonian models should always be used to perform 3D FSI simulations of blood flow; we simply state that there is a difference in the results that we must be aware of when a model for blood flow is chosen. Ultimately, there is a need for experimental results to establish if the flow conditions necessary for triggering non-Newtonian effects in blood are present *in vivo*, in the vascular region under consideration.

References

[1] C.J.L. Murray, D.A. Lopez, The global burden of disease. The Harvard School of Public Health and World Health Organization and World Bank, 1996.
[2] L. Formaggia, A. Quarteroni, A. Veneziani (Eds.), Cardiovascular Mathematics. Modeling and Simulation of the Circulatory System, in: MS & A, vol. 1, Springer, 2009.
[3] A. Robertson, A. Sequeira, M. Kameneva, Hemorheology, in: G.P. Galdi, R. Rannacher, A. Robertson, S. Turek (Eds.), Haemodynamical Flows: Modelling Analysis and Simulation, in: Oberwolfach Seminars, vol. 37, Birkhauser, 2008, pp. 63–120.

[4] F.J.H. Gijsen, E. Allanic, F.N. van de Vosse, J.D. Janssen, The influence of the non-Newtonian properies of blood on the flow in large arteries: Unsteady flow in a 90° curved tube, J. Biomech. 32 (1999) 705–713.
[5] A.M. Robertson, A. Sequeira, R.G. Owens, Rheological models for blood, in: A. Quarteroni, L. Formaggia, A. Veneziani (Eds.), Cardiovascular Mathematics. Modeling and Simulation of the Cardiovascular System, in: MS & A, vol. 1, Spriger-Verlag, 2009.
[6] J. Janela, Mathematical and numerical modelling in hemodynamics and hemorheology, Ph.D. Thesis, Instituto Superior Técnico, 2008.
[7] P. Causin, J.-F. Gerbeau, F. Nobile, Added-mass effect in the design of partitioned algorithms for fluid-structure problems, Comput. Methods Appl. Mech. Engrg. 194 (2005) 4506–4527.
[8] M.A. Fernández, M. Moubachir, A Newton method using exact Jacobian for solving fluid-structure coupling, Comput. Struct. 83 (2–3) (2005) 127–142.
[9] L. Formaggia, A. Moura, F. Nobile, On the stability of the coupling of 3D and 1D fluid-structure interaction models for blood flow simulations, Math. Modelling Numer. Anal. 41 (4) (2007) 743–769.
[10] B.R. Bird, R.C. Armstrong, O. Hassager, Dynamics of Polymeric Liquids, John Wiley & Sons, 1987.
[11] Y.I. Cho, K.R. Kensey, Effects of the non-Newtonian viscosity of blood on flows in a diseased arterial vessel. Part I: Steady flows, Biorheology 28 (1991) 241–262.
[12] A. Moura, The geometrical multiscale modelling of the cardiovascular system: Coupling 3D and 1D models, Ph.D. Thesis, Politecnico di Milano, 2007.
[13] Y.C. Fung, Mechanical Properties of Living Tissues. Biomechanics, second ed., Springer, 1993.
[14] G.A. Holzapfel, T. Gasser, R. Ogden, A new constitutive framework for arterial wall mechanics and a comparative study of material models, J. Elasticity 61 (2000) 1–48.
[15] P.G. Ciarlet, Mathematical Elasticity. Volume 1: Three Dimensional Elasticity, second ed., Elsevier, 2004.
[16] A. Chambolle, B. Desjardins, M. Esteban, C. Grandmont, Existence of weak solutions for the unsteady interaction of a viscous fluid with an elastic plate, J. Math. Fluid Mech. 7 (2005) 368–404.
[17] H. Beirão da Veiga, On the existence of strong solutions to a coupled fluid-structure evolution problem, J. Math. Fluid Mech. 6 (2004) 21–52.
[18] D. Coutand, S. Shkoller, The interaction between quasilinear elastodynamics and the Navier–Stokes equations, Arch. Ration. Mech. Anal. 179 (2006) 303–352.
[19] T.E. Tezduyar, Finite element methods for fluid dynamics with moving boundaries and interfaces, Arch. Comput. Methods Eng. 8 (2001) 83–130.
[20] L. Formaggia, F. Nobile, A stability analysis for the arbitrary Lagrangian Eulerian formulation with finite elements, East–West J. Numer. Math. 7 (1999) 105–132.
[21] P. Hansbo, A. Szepessy, A velocity–pressure streamline diffusion finite element method for the incompressible Navier–Stokes equations, Comput. Methods Appl. Mech. Engrg. 84 (2) (1990) 175–192.
[22] L. Tobiska, R. Verfürth, Analysis of a streamline diffusion finite element method for the Stokes and Navier–Stokes equations, SIAM J. Numer. Anal. 33 (1) (1996) 107–127.
[23] S. Kim, Y.I. Cho, A.H. Jeon, B. Hogenauer, K.R. Kensey, A new method for blood viscosity measurements, J. Non-Newton. Fluid Mech. 94 (2000) 47–56.